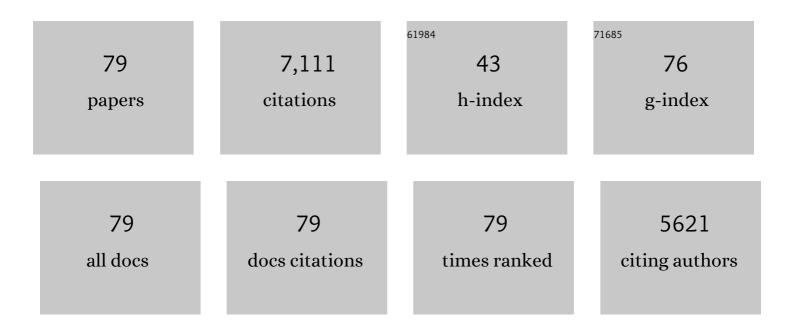
List of Publications by Year in descending order

Source: https://exaly.com/author-pdf/2870675/publications.pdf Version: 2024-02-01



XIN HUANC

#	Article	IF	CITATIONS
1	A framework for assessing the systemic risk of major financial institutions. Journal of Banking and Finance, 2009, 33, 2036-2049.	2.9	509
2	An SVM Ensemble Approach Combining Spectral, Structural, and Semantic Features for the Classification of High-Resolution Remotely Sensed Imagery. IEEE Transactions on Geoscience and Remote Sensing, 2013, 51, 257-272.	6.3	389
3	On Combining Multiple Features for Hyperspectral Remote Sensing Image Classification. IEEE Transactions on Geoscience and Remote Sensing, 2012, 50, 879-893.	6.3	367
4	Morphological Building/Shadow Index for Building Extraction From High-Resolution Imagery Over Urban Areas. IEEE Journal of Selected Topics in Applied Earth Observations and Remote Sensing, 2012, 5, 161-172.	4.9	315
5	Multiple Feature Learning for Hyperspectral Image Classification. IEEE Transactions on Geoscience and Remote Sensing, 2015, 53, 1592-1606.	6.3	282
6	Ensemble manifold regularized sparse low-rank approximation for multiview feature embedding. Pattern Recognition, 2015, 48, 3102-3112.	8.1	260
7	Tensor Discriminative Locality Alignment for Hyperspectral Image Spectral–Spatial Feature Extraction. IEEE Transactions on Geoscience and Remote Sensing, 2013, 51, 242-256.	6.3	251
8	Systemic Risk Contributions. Journal of Financial Services Research, 2012, 42, 55-83.	1.5	231
9	An Adaptive Mean-Shift Analysis Approach for Object Extraction and Classification From Urban Hyperspectral Imagery. IEEE Transactions on Geoscience and Remote Sensing, 2008, 46, 4173-4185.	6.3	210
10	Processing of Multiresolution Thermal Hyperspectral and Digital Color Data: Outcome of the 2014 IEEE GRSS Data Fusion Contest. IEEE Journal of Selected Topics in Applied Earth Observations and Remote Sensing, 2015, 8, 2984-2996.	4.9	193
11	A pixel shape index coupled with spectral information for classification of high spatial resolution remotely sensed imagery. IEEE Transactions on Geoscience and Remote Sensing, 2006, 44, 2950-2961.	6.3	186
12	Sparse Transfer Manifold Embedding for Hyperspectral Target Detection. IEEE Transactions on Geoscience and Remote Sensing, 2014, 52, 1030-1043.	6.3	173
13	Hyperspectral Remote Sensing Image Subpixel Target Detection Based on Supervised Metric Learning. IEEE Transactions on Geoscience and Remote Sensing, 2014, 52, 4955-4965.	6.3	171
14	Classification and Extraction of Spatial Features in Urban Areas Using High-Resolution Multispectral Imagery. IEEE Geoscience and Remote Sensing Letters, 2007, 4, 260-264.	3.1	154
15	Compression of hyperspectral remote sensing images by tensor approach. Neurocomputing, 2015, 147, 358-363.	5.9	154
16	The systemic risk of European banks during the financial and sovereign debt crises. Journal of Banking and Finance, 2016, 63, 107-125.	2.9	147
17	Unsupervised Feature Learning Via Spectral Clustering of Multidimensional Patches for Remotely Sensed Scene Classification. IEEE Journal of Selected Topics in Applied Earth Observations and Remote Sensing, 2015, 8, 2015-2030.	4.9	145
18	A multi-index learning approach for classification of high-resolution remotely sensed images over urban areas. ISPRS Journal of Photogrammetry and Remote Sensing, 2014, 90, 36-48.	11.1	137

#	Article	IF	CITATIONS
19	Building Change Detection From Multitemporal High-Resolution Remotely Sensed Images Based on a Morphological Building Index. IEEE Journal of Selected Topics in Applied Earth Observations and Remote Sensing, 2014, 7, 105-115.	4.9	136
20	Road centreline extraction from highâ€resolution imagery based on multiscale structural features and support vector machines. International Journal of Remote Sensing, 2009, 30, 1977-1987.	2.9	132
21	Assessing the systemic risk of a heterogeneous portfolio of banks during the recent financial crisis. Journal of Financial Stability, 2012, 8, 193-205.	5.2	132
22	Support Tensor Machines for Classification of Hyperspectral Remote Sensing Imagery. IEEE Transactions on Geoscience and Remote Sensing, 2016, 54, 3248-3264.	6.3	131
23	The Flexible Global Oceanâ€Atmosphere‣and System Model Gridâ€Point Version 3 (FGOALSâ€g3): Description and Evaluation. Journal of Advances in Modeling Earth Systems, 2020, 12, e2019MS002012.	3.8	129
24	Evaluation of Morphological Texture Features for Mangrove Forest Mapping and Species Discrimination Using Multispectral IKONOS Imagery. IEEE Geoscience and Remote Sensing Letters, 2009, 6, 393-397.	3.1	102
25	A comparative study of spatial approaches for urban mapping using hyperspectral ROSIS images over Pavia City, northern Italy. International Journal of Remote Sensing, 2009, 30, 3205-3221.	2.9	101
26	Combining Pixel- and Object-Based Machine Learning for Identification of Water-Body Types From Urban High-Resolution Remote-Sensing Imagery. IEEE Journal of Selected Topics in Applied Earth Observations and Remote Sensing, 2015, 8, 2097-2110.	4.9	100
27	Hyperspectral image noise reduction based on rank-1 tensor decomposition. ISPRS Journal of Photogrammetry and Remote Sensing, 2013, 83, 50-63.	11.1	96
28	A Multichannel Gray Level Co-Occurrence Matrix for Multi/Hyperspectral Image Texture Representation. Remote Sensing, 2014, 6, 8424-8445.	4.0	88
29	Wavelength selection and spectral discrimination for paddy rice, with laboratory measurements of hyperspectral leaf reflectance. ISPRS Journal of Photogrammetry and Remote Sensing, 2011, 66, 672-682.	11.1	87
30	Spatiotemporal Detection and Analysis of Urban Villages in Mega City Regions of China Using High-Resolution Remotely Sensed Imagery. IEEE Transactions on Geoscience and Remote Sensing, 2015, 53, 3639-3657.	6.3	87
31	New Postprocessing Methods for Remote Sensing Image Classification: A Systematic Study. IEEE Transactions on Geoscience and Remote Sensing, 2014, 52, 7140-7159.	6.3	85
32	A Novel Automatic Change Detection Method for Urban High-Resolution Remotely Sensed Imagery Based on Multiindex Scene Representation. IEEE Transactions on Geoscience and Remote Sensing, 2016, 54, 609-625.	6.3	77
33	Information fusion of aerial images and LIDAR data in urban areas: vector-stacking, re-classification and post-processing approaches. International Journal of Remote Sensing, 2011, 32, 69-84.	2.9	73
34	A Multifeature Tensor for Remote-Sensing Target Recognition. IEEE Geoscience and Remote Sensing Letters, 2011, 8, 374-378.	3.1	68
35	The Recent Decline and Recovery of Indian Summer Monsoon Rainfall: Relative Roles of External Forcing and Internal Variability. Journal of Climate, 2020, 33, 5035-5060.	3.2	65
36	Fault-Tolerant Building Change Detection From Urban High-Resolution Remote Sensing Imagery. IEEE Geoscience and Remote Sensing Letters, 2013, 10, 1060-1064.	3.1	63

#	Article	IF	CITATIONS
37	South Asian summer monsoon projections constrained by the interdecadal Pacific oscillation. Science Advances, 2020, 6, eaay6546.	10.3	58
38	Multiple Morphological Component Analysis Based Decomposition for Remote Sensing Image Classification. IEEE Transactions on Geoscience and Remote Sensing, 2016, 54, 3083-3102.	6.3	56
39	Multiple Morphological Profiles From Multicomponent-Base Images for Hyperspectral Image Classification. IEEE Journal of Selected Topics in Applied Earth Observations and Remote Sensing, 2014, 7, 4653-4669.	4.9	53
40	Object-Based 3-D Building Change Detection on Multitemporal Stereo Images. IEEE Journal of Selected Topics in Applied Earth Observations and Remote Sensing, 2015, 8, 2125-2137.	4.9	50
41	Classification of Ultra-High Resolution Orthophotos Combined with DSM Using a Dual Morphological Top Hat Profile. Remote Sensing, 2015, 7, 16422-16440.	4.0	49
42	An Adaptive Multiscale Information Fusion Approach for Feature Extraction and Classification of IKONOS Multispectral Imagery Over Urban Areas. IEEE Geoscience and Remote Sensing Letters, 2007, 4, 654-658.	3.1	48
43	Automatic Labelling and Selection of Training Samples for High-Resolution Remote Sensing Image Classification over Urban Areas. Remote Sensing, 2015, 7, 16024-16044.	4.0	45
44	Quality Assessment of Panchromatic and Multispectral Image Fusion for the ZY-3 Satellite: From an Information Extraction Perspective. IEEE Geoscience and Remote Sensing Letters, 2014, 11, 753-757.	3.1	39
45	Generalized Differential Morphological Profiles for Remote Sensing Image Classification. IEEE Journal of Selected Topics in Applied Earth Observations and Remote Sensing, 2016, 9, 1736-1751.	4.9	39
46	Three-Dimensional Wavelet Texture Feature Extraction and Classification for Multi/Hyperspectral Imagery. IEEE Geoscience and Remote Sensing Letters, 2014, 11, 2183-2187.	3.1	38
47	Macroeconomic news announcements, systemic risk, financial market volatility, and jumps. Journal of Futures Markets, 2018, 38, 513-534.	1.8	37
48	Object-oriented subspace analysis for airborne hyperspectral remote sensing imagery. Neurocomputing, 2010, 73, 927-936.	5.9	36
49	Dynamic texture recognition by aggregating spatial and temporal features via ensemble SVMs. Neurocomputing, 2016, 173, 1310-1321.	5.9	35
50	Joint Collaborative Representation With Multitask Learning for Hyperspectral Image Classification. IEEE Transactions on Geoscience and Remote Sensing, 2014, 52, 5923-5936.	6.3	34
51	Comparison of Vector Stacking, Multi-SVMs Fuzzy Output, and Multi-SVMs Voting Methods for Multiscale VHR Urban Mapping. IEEE Geoscience and Remote Sensing Letters, 2010, 7, 261-265.	3.1	33
52	Object-oriented change detection based on the Kolmogorov–Smirnov test using high-resolution multispectral imagery. International Journal of Remote Sensing, 2011, 32, 5719-5740.	2.9	33
53	A modified stochastic neighbor embedding for multi-feature dimension reduction of remote sensing images. ISPRS Journal of Photogrammetry and Remote Sensing, 2013, 83, 30-39.	11.1	33
54	Improving Backscatter Intensity Calibration for Multispectral LiDAR. IEEE Geoscience and Remote Sensing Letters, 2015, 12, 1421-1425.	3.1	33

#	Article	IF	CITATIONS
55	Feature Extraction of Hyperspectral Images With Semisupervised Graph Learning. IEEE Journal of Selected Topics in Applied Earth Observations and Remote Sensing, 2016, 9, 4389-4399.	4.9	31
56	A Novel MRF-Based Multifeature Fusion for Classification of Remote Sensing Images. IEEE Geoscience and Remote Sensing Letters, 2016, 13, 515-519.	3.1	30
57	A Morphological Building Detection Framework for High-Resolution Optical Imagery Over Urban Areas. IEEE Geoscience and Remote Sensing Letters, 2016, 13, 1388-1392.	3.1	25
58	Classification of hyperspectral urban data using adaptive simultaneous orthogonal matching pursuit. Journal of Applied Remote Sensing, 2014, 8, 085099.	1.3	24
59	Assessing the Systemic Risk of a Heterogeneous Portfolio of Banks during the Recent Financial Crisis. SSRN Electronic Journal, 0, , .	0.4	22
60	A multilevel decision fusion approach for urban mapping using very high-resolution multi/hyperspectral imagery. International Journal of Remote Sensing, 2012, 33, 3354-3372.	2.9	22
61	Systemic Risk Contributions. SSRN Electronic Journal, 0, , .	0.4	19
62	A multiscale urban complexity index based on 3D wavelet transform for spectral–spatial feature extraction and classification: an evaluation on the 8-channel WorldView-2 imagery. International Journal of Remote Sensing, 2012, 33, 2641-2656.	2.9	19
63	A Novel Clustering-Based Feature Representation for the Classification of Hyperspectral Imagery. Remote Sensing, 2014, 6, 5732-5753.	4.0	18
64	Thermal Conductivity Reduction in a Silicon Thin Film with Nanocones. ACS Applied Materials & Interfaces, 2019, 11, 34394-34398.	8.0	17
65	A novel building change index for automatic building change detection from high-resolution remote sensing imagery. Remote Sensing Letters, 2014, 5, 713-722.	1.4	15
66	Northern Hemisphere land monsoon precipitation changes in the twentieth century revealed by multiple reanalysis datasets. Climate Dynamics, 2019, 53, 7131-7149.	3.8	12
67	Assessing and Improving the Accuracy of GlobeLand30 Data for Urban Area Delineation by Combining Multisource Remote Sensing Data. IEEE Geoscience and Remote Sensing Letters, 2016, 13, 1860-1864.	3.1	10
68	Coherent and Incoherent Impacts of Nanopillars on the Thermal Conductivity in Silicon Nanomembranes. ACS Applied Materials & Interfaces, 2020, 12, 25478-25483.	8.0	10
69	An Energy-Driven Total Variation Model for Segmentation and Classification of High Spatial Resolution Remote-Sensing Imagery. IEEE Geoscience and Remote Sensing Letters, 2013, 10, 125-129.	3.1	9
70	Fully Constrained Least Squares for Antarctic Sea Ice Concentration Estimation Utilizing Passive Microwave Data. IEEE Geoscience and Remote Sensing Letters, 2015, 12, 2291-2295.	3.1	8
71	A Fully Automatic Method to Extract Rare Earth Mining Areas from Landsat Images. Photogrammetric Engineering and Remote Sensing, 2016, 82, 729-737.	0.6	8
72	A structural similarity-based label-smoothing algorithm for the post-processing of land-cover classification. Remote Sensing Letters, 2016, 7, 437-445.	1.4	8

#	Article	IF	CITATIONS
73	Simulation of Low-Resolution Panchromatic Images by Multivariate Linear Regression for Pan-Sharpening IKONOS Imageries. IEEE Geoscience and Remote Sensing Letters, 2010, 7, 515-519.	3.1	7
74	The Systemic Risk of European Banks During the Financial and Sovereign Debt Crises. SSRN Electronic Journal, 2012, , .	0.4	7
75	Classification of high-spatial resolution imagery based on distance-weighted Markov random field with an improved iterated conditional mode method. International Journal of Remote Sensing, 2011, 32, 9843-9868.	2.9	4
76	Generalization of spectral fidelity with flexible measures for the sparse representation classification of hyperspectral images. International Journal of Applied Earth Observation and Geoinformation, 2016, 52, 275-283.	2.8	4
77	The risk of betting on risk: Conditional variance and correlation of bank credit default swaps. Journal of Futures Markets, 2020, 40, 710-721.	1.8	4
78	Persistence of Bank Credit Default Swap Spreads. Risks, 2019, 7, 90.	2.4	3
79	Foreword to the Special Issue on Information Extraction From High-Spatial-Resolution Optical Remotely Sensed Imagery. IEEE Journal of Selected Topics in Applied Earth Observations and Remote Sensing, 2015, 8, 1872-1875.	4.9	0